

# Spatial-Temporal Variability of UV-Absorbing Aerosol Index over Egypt

Eman F. El-Nobi

Atmospheric Physics Lab., Physics Dep.  
Faculty of Science, South Valley University  
Qena, Egypt  
eman.fouad@sci.svu.edu.eg

**Abstract**—The ultraviolet absorbing Aerosol Index observations derived from the Ozone Monitoring Instrument (OMI-AI) are analyzed over Egypt covering the geographical domain (22°–31°N, 24°–36°E) during the period from 2005 to 2016. In the temporal variability, time series, daily, monthly average variation of OMI-AI and its frequency distributions, represent threshold, were created. Time series values reflect increase with the time, with increasing rate equal to  $0.7 \times 10^{-4}$ . In the spatial distribution, with a spatial resolution of  $1^\circ \times 1^\circ$ , OMI-AI value used to reveal the west to east decreasing gradient. Therefore, the relationships between daily OMI-AI and longitude (Lon), in mean-latitude (27.5°N), with inverse correlation have examined. The correlation coefficient  $R^2$  in cold season, hot season and all period values are 40%, 32% and 29% respectively.

**Keywords**— *Temporal variability; Contour maps; OMI data; UV-absorbing aerosol index; Egypt.*

## I. INTRODUCTION

Since thirteen years ago, a new expression of the ultraviolet absorbing aerosol index (AAI) was introduced to be more sensitive to ultraviolet absorbing aerosols. This aerosol index depends on measurements of the reflectance at different two wavelengths in the ultraviolet coupled with radiative transfer model of the Rayleigh atmosphere. At first, the Total Ozone Mapping Spectrometer (TOMS) developed it but after that it was adapted for use with the Ozone Monitoring Instrument (OMI), also it called Aerosol index (AI).

It is a helpful parameter for deducing the existence of near ultraviolet absorbing aerosols in the earth's atmosphere such as smoke, mineral dust or soot, desert dust, and volcanic ash, cloud, no indication of sulfate aerosols. As well as, studying the aerosol behavior in the energy budget and climate forcing, since it allows characterize the spatial distributions and temporal variation of tropospheric aerosols over both oceans and land surface [1-5].

The existence of ultraviolet absorbing aerosols in the earth's atmosphere affects the amount of ultraviolet radiation reaching the earth's surface and the radiation balance. The atmospheric loading of ultraviolet absorbing aerosols is the sum of several large

annually cyclic sources of aerosols distributed over large areas by tropospheric wind circulation [6],[7]. Observations of ultraviolet absorbing aerosols at sites remote from the sources also show a distinct cyclic pattern [8] driven by atmospheric transport from one or more of these sources. The greatest sources of ultraviolet absorbing aerosols in the earth's atmosphere are from biomass burning and wind-borne desert dust from events that last a week or longer [2].

There are three reasons that make AAI such a helpful index are: (1) It is not more sensitive to surface type, which allows retrieval over both oceans and land by the same algorithm. (2) The AAI can be retrieved in the presence of clouds, and is in fact even more susceptible to absorbing aerosols above strongly reflective surfaces such as clouds, snow and ice [3, 9-10]. (3) The AAI contains information about aerosol layer height [2-3,11-14].

In spite of that the Ozone Monitoring Instrument absorbing Aerosol Index (OMI-AI) is an indicator of the presence of the absorbing aerosols in the earth's atmosphere, does not measure actual concentration of dust, many scientists have used, very useful, in being widely used to increasingly for variety of applications, for instance to: (1) Detection , monitoring the propagation of soil dust in the atmosphere [2,15-17] and identified dust source regions at global scale [15, 18- 21] also, understanding the transport of desert dust [2,12,14]. (2) Monitoring dust activities of retrieving aerosol properties over land surface and a sign for the existence of dust for a dust storm intense [2-3, 21-22]. (3) Studied the nature and consequences characterize the dust sources of Saharan dust [20,15,18, 23] and detected key source areas of dust plume in the whole world [18,24-25]. (4) Mapping global distribution of ultraviolet absorbing aerosols correcting for aerosol-induced errors in the retrieval of column ozone amounts [2]. (5) Identifying the sources of air pollution (identify carbon and mineral aerosols from pure scattering particles such as sulphate aerosol and sea salt aerosol) over the whole globe and understanding the transport of air pollution across the oceans and continents [1-2, 9, 14, 25-32]. (6) Study radiation energy balance, climate forcing and air quality forecast models such as model air quality and forecast [33-34].

Till now ultraviolet absorbing aerosols driven from OMI satellite (OMI-AI) is not yet sufficiently described over Egypt. This study analyzes the spatial-temporal of OMI-AI and its distribution over Egypt covering the geographical area 22°–31°N, 24°–36°E during the

period from 2005 to 2016. Many studies have been made to understand the chief reasons for the increased pollution levels in Cairo using both ground-based and satellite air quality data, for example, [35-46].

This study analyzes OMI-AI over Egypt, a poorly studied area, and having locations with a variation of ultraviolet aerosol index patterns, covering the geographical area 22°–31°N, 24°–36°E during the period (2005-2016). The chief objective goal of this study is double. In the first part of this study, we present an overview of OMI-AI, in 1 pixel, for whole Egypt territory. The second goal of this work is to study the regional spatial distribution of absorbing aerosols with a spatial resolution of 1°×1°, 104 pixels, for whole Egypt territory. To the best of our knowledge no such study has so far been used to analyze the variability of OMI-AI over Egypt obtained from OMI. To study the effect of longitude on variation of absorbing aerosol loading, we have also found its correlation with the OMI-AI measurements.

We briefly description of the remote sensing instruments used in this work and give a short explanation of the algorithm chosen for data product in Section II. Section III is the analysis and discussion of the results, subdivided into two parts. The first part analyzes the OMI-AI climatology (temporal variability including the time series, daily and monthly average variation of OMI-AI), the second part targets the evaluation of the spatial distribution; follow by its relationship with the longitude. Finally, main concluding points of the paper presented in Section IV.

## II. OMI UV AEROSOL INDEX DATA ACCESS

The Ozone Monitoring Instrument (OMI) flown onboard the NASA EOS Aura spacecraft (propelled July 2004) [47]. OMI is the successor of the TOMS instruments, The key targets of the OMI estimations incorporate monitoring of the Earth's ozone, aerosols, air quality, and smokes from biomass burning, SO<sub>2</sub> from volcanic ejections, and key tropospheric pollutants and surface UV radiation. It gauges the sun oriented light scattered by the atmosphere in the 270–500 nm wavelength scope of the sun spectrum. In view of better estimation accuracy and better spatial resolution (changing from 13 km × 24 km at nadir to around 28 km × 150 km along its scan edges) OMI gives better gauges of atmospheric pollutants and their vehicle through the Earth's environment [47-49].

The OMI estimations are utilized as contribution to reversal calculations to recover ozone column amount and its vertical distribution, clouds, aerosols, and total column amounts of the trace gases SO<sub>2</sub>, NO<sub>2</sub>, OClO, BrO, and HCHO. Torres et al. [4] described in detail (OMAERUV) algorithm. The NASA Goddard Earth Sciences Data and Information Services Center (GES DISC) has developed a web based on line data visualization and data mining capabilities called 'Giovanni'. The Giovanni (GES-DISC Interactive On-line Visualization & Analysis Infrastructure) is a Web based interface for data exploration, visualization and analysis (<https://giovanni.gsfc.nasa.gov/>).

The UV Aerosol record (AI) is a measure of how much the wavelength reliance of backscattered UV radiation, where the ozone absorption is very small, from an air containing aerosols (absorption, Rayleigh scattering and Mie scattering) differs from that of a pure molecular atmosphere (pure Rayleigh scattering). It is the difference between the observations and model calculations of absorbing and non-absorbing spectral radiance ratios. Quantitatively, the aerosol index AI is defined to be

$$AI = 100 \left[ \log_{10} \left( \frac{I_{360}}{I_{331}} \right)_{meas} - \log_{10} \left( \frac{I_{360}}{I_{331}} \right)_{calc} \right] \quad (1)$$

where  $I_{meas}$  is the measured backscattered radiance at a given wavelength and  $I_{calc}$  is the backscattered radiance calculated at that wavelength for a pure Rayleigh atmosphere [4]. Thus by this methodology, AI positive values, AI >1, are generally represent UV-absorbing aerosols such as carbonaceous aerosols, soot particles, volcanic ash aerosols, mineral dust and smoke. However, negative values, AI <0, are associated with non-absorbing aerosols (pure scattering) such as sulfate and sea salt particles from both natural and anthropogenic sources since the AI increases with altitude for the same aerosol load [3,15]. Near zero, AI=0, values represent cloud presence [11,21, 34, 45, 49-50].

## III. RESULTS AND DISCUSSION

### A. Temporal Variation of OMI-AI

In the frame of the variability, Egypt which covering the geographical domain (22°–31°N, 24°–36°E) was considered as an average area (one pixel). Variations of OMI-AI during the studied period (2005-2016) time series, daily, monthly average variation and its frequency distributions, represent threshold, were created for cold seasons, hot seasons and all period.

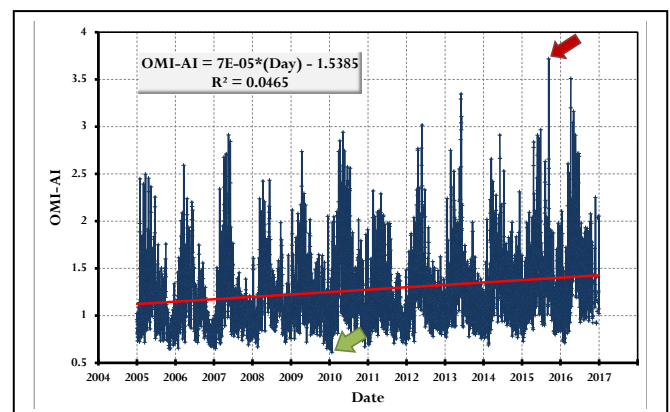


Fig. 1. Time series variations of OMI-AI over Egypt during the studied period, red line introduce the trend, Maximum value in 2015 (red narrow) while the minimum value in 2010 (green narrow).

Fig. 1 shows the daily time series of OMI-AI over whole Egypt, the values reflect increase with the time, with increasing rate of OMI-AI equal to  $0.7 \times 10^{-4}$ . Maximum was 3.72 occurrences in 10th September 2015 and Minimum was 0.61 occurrences in 25<sup>th</sup> January 2010. Fig. 2 shows daily average variation of

OMI-AI over whole Egypt, during the studied period. OMI-AI has generally high values during hot seasons, spring and summer, and low values during cold seasons, winter and autumn. The maximum daily average values were  $2.01 \pm 0.62$ , while the minimum daily average values were  $0.86 \pm 0.09$ . Standard deviations (vertical lines) of daily average values have generally high values during hot season's days reaching  $\pm 0.76$ . But its value decreasing to  $\pm 0.03$  at cold season's days, i.e. these values were more fluctuate in hot season. It may be attributed to the weather conditions. The relatively high temperature in hot season's days, this leads to encouragement of air convection and up-word movement of air parcels containing aerosols. Effect of Khamsin depression which lead to increasing of dust storms occurrence. Fig. 3 shows the time series of monthly mean variations of OMI-AI with their corresponding standard deviations over Egypt during the studied period. The OMI-AI values ranged from 0.79 up to 1.82. The OMI-AI variability in the same month changes lightly from year-to-year, characterized by yearly cyclic variations, with highest values viewed in the hot months (March–August), while lowest values were recorded during cold months (September–February) with increasing trend equal to  $0.6 \times 10^{-5}$  for the studied period.

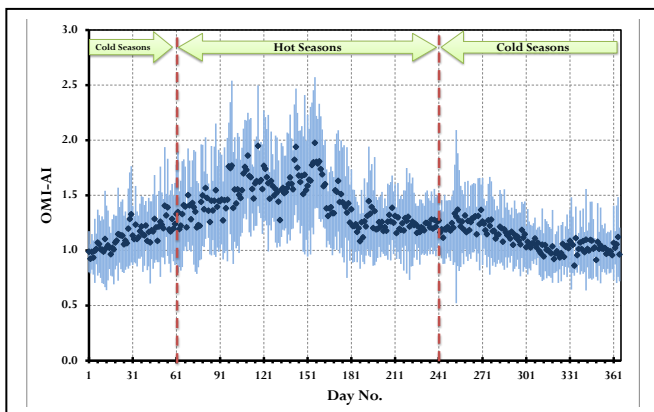


Fig. 2. Daily average variations of OMI-AI, vertical lines (standard deviation), over Egypt during the studied period.

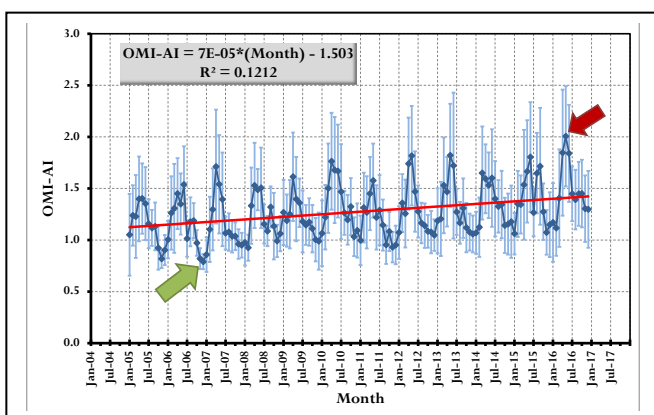


Fig. 3. The time series of mean monthly variation of OMI-AI with the standard deviation, error bars, the trend in values over Egypt is shown by linear fit (red line).

Hot months show relatively high monthly average values of OMI-AI compared with the corresponding

value in cold months. It may be ascribed to the weather conditions. The maximum average value of OMI-AI recorded in May 2013, it was 1.82 while the minimum value recorded in December 2006, and it was 0.79.

### B. Box and Whiskers diagrams

Fig. 4 summarizes the statistics of monthly values of OMI-AI; Box and Whiskers diagrams have been used to illuminate the characteristics of the OMI-AI data. Here, we notice a significant increasing trend in all computed results (average for example) OMI-AI increases from January (1.07) to April (1.60) and then remains almost constant up to June (1.52) followed by a gradual decrease up to December (1.02). These average monthly variations in OMI-AI over Egypt can be well justified by considering the cyclic variations in meteorological conditions and anthropogenic. Box and Whiskers diagrams of yearly values of OMI-AI; shown in Fig. 5, we notice (maximum for example) OMI-AI in 2016 have the high record (2.36) and followed by 2010 (2.20).

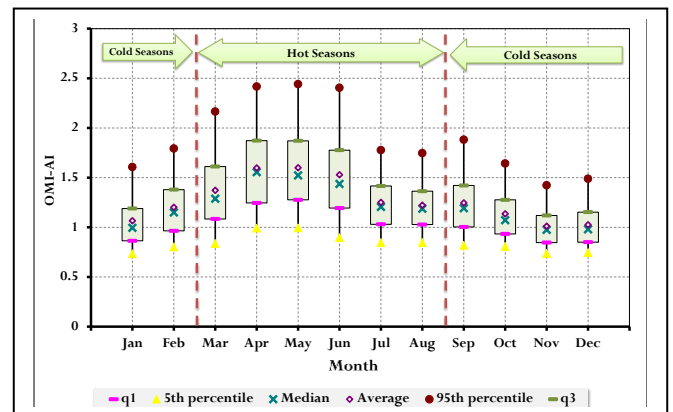


Fig. 4. The monthly box-whisker plots for OMI-AI over Egypt.

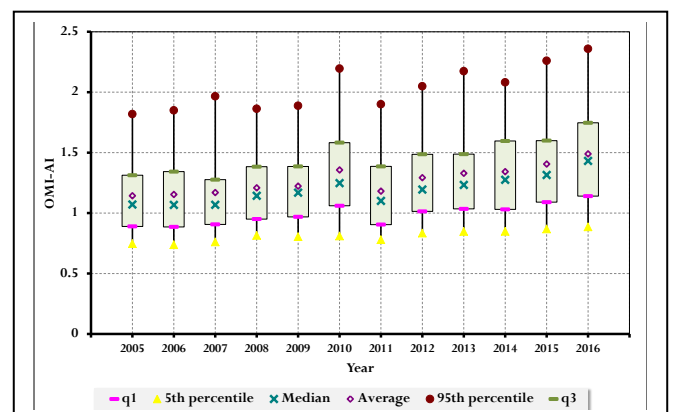


Fig. 5. The yearly box-whisker plots for OMI-AI over Egypt.

### C. Threshold frequency distributions of OMI-AI

Some researchers have studied thresholds in order to reduce possible bias in the analysis of AI data and determine dust sources underestimate the importance of sources on the edges of deserts [12, 51]. Thresholds are varying introduced which set at 1.0 over North Africa, the Middle East and South and Central Asia, and 0.7 over all other areas [15, 25].

Fig. 6 illustrates Gaussian distribution of seasonal OMI-AI over Egypt; the dashed vertical red line represents threshold line, in this paper, we use 1.0 as the threshold. The distribution is more directed to low values in the cold seasons in comparison with that in hot one which characterized by relatively high pollutant.

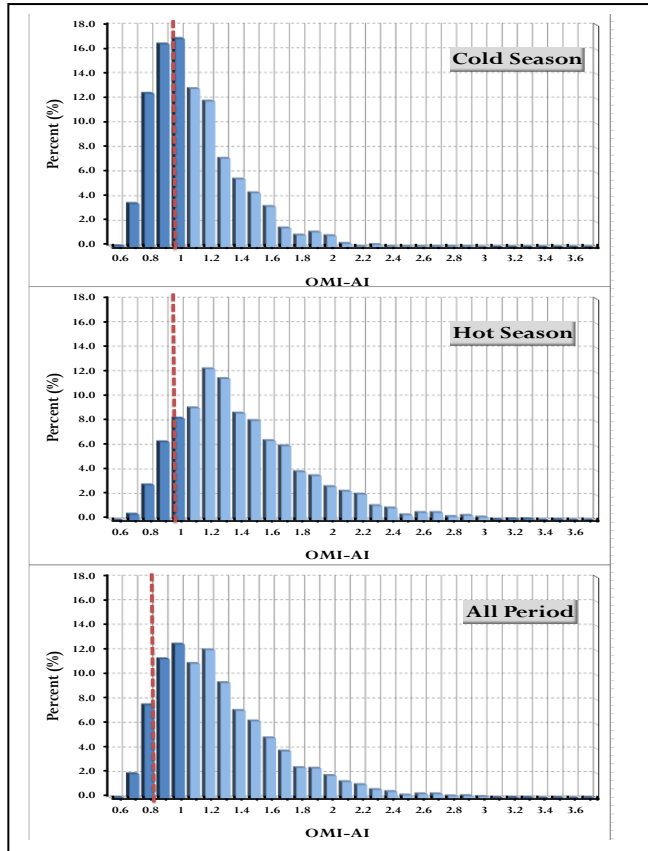


Fig. 6. Threshold frequency distributions of cold season, hot season and all period OMI-AI over Egypt; use 1.0 as the threshold, represent by the dashed vertical red line.

#### D. Spatial distribution of OMI-AI

About 12-years (2005 to 2016) daily OMI-AI average spatial distribution over Egypt is mapped onto a grid of 1° in longitude by 1° in latitude shown in Fig. 7 to Fig. 9. The cold season recorded the minimum values of OMI-AI, because of the increased amount of rainfall and high relative humidity leading to aerosol size increases and subsequent deposition over Egypt, as shown in Fig. 7. Also, decreases in temperature, leading to high water uptake in the aerosols, hence increased particle size and mass, and increased fall and deposition velocities. In Hot season, The Mediterranean is frequently impacted by dust storms in the late spring and summer [52- 53]. The TOMS data suggest that the principal sources of the dust are most likely the regions described here in eastern Algeria, Tunisia, Libya, and Egypt [15]. In the cold seasons the values, indicating a decreasing trend of OMI-AI. This leads to an overall mean increasing OMI-AI of  $0.015 \pm 0.148$  and  $0.032 \pm 0.165$  for the cold and the hot season, respectively. The remarkable finding in this

season is the highest OMI-AI values as well as the strong east-to-west gradient.

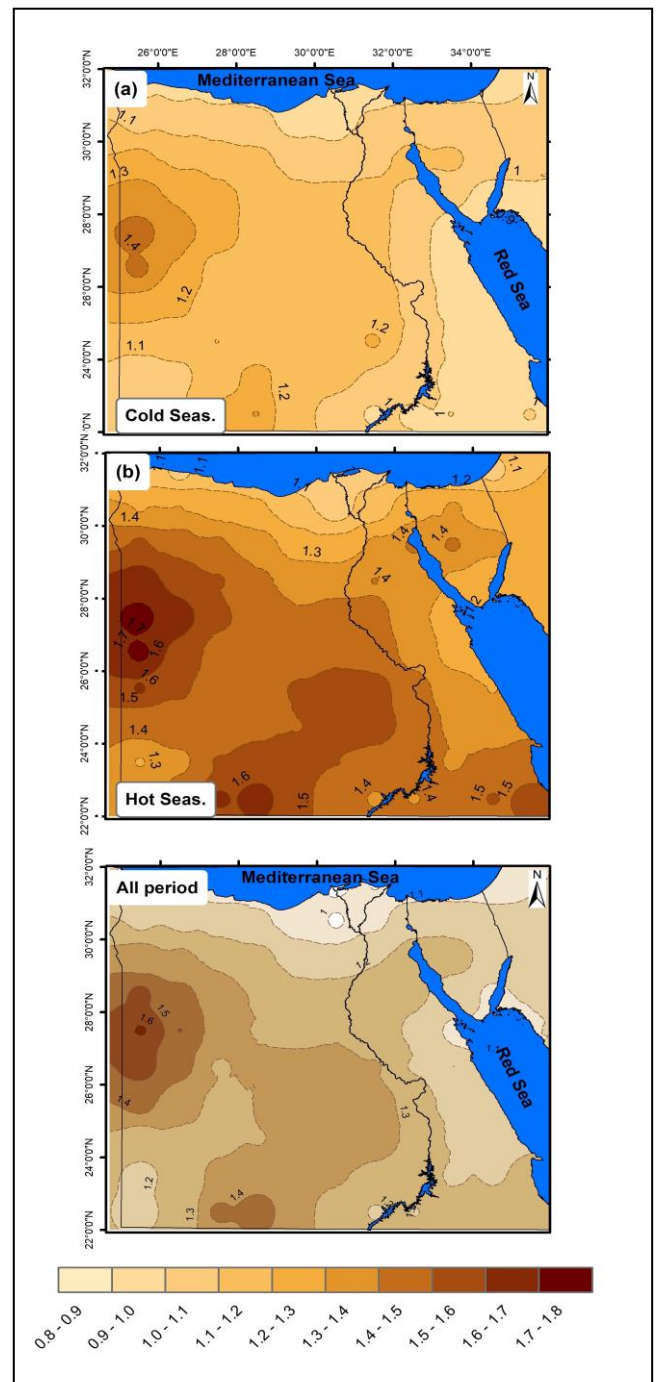


Fig. 7. Spatial distribution of average OMI-AI for a) cold season b) hot season and all period over Egypt (2005 to 2016).

Notice That OMI-AI has a periodic and seasonal behavior; the increase of OMI-AI values (1.9–2.0) mainly in March to June are found over the northwest regions of Egypt (Fig. 8), directly affected by the existence of dust particles still suspended in the air at Libya desert. May exhibits higher values over all parts of Egypt with emphasis in the north-west. OMI-AI decreases in cold months, while values equal to those of December are observed only on certain days. Furthermore, in hot season, the aforementioned situation strongly changes. Significant seasonal

differences are revealed in both OMI-AI values and their spatial distribution over Egypt. In hot season the maximum dust transport occurs in North Africa when large quantities of dust are carried across the Mediterranean to Europe and the Middle East [52] and across the Atlantic to the Caribbean [54], the southeastern United States [55-56], and the midlatitude western North Atlantic [15]. In contrast, frequent chained depressions can be observed in spring, These depressions, called "Khamsein"

depressions in Arabic, coincide with strong winds blowing from the south/southwest and raising dust on their way [42, 57]. Fig. 9, illustrate the annual distribution, shows a significant match in spatial distribution from year to another. So we can say that the distribution of aerosols on Egypt annually is almost constant in terms of distribution but differs slightly in terms of value; The highest values recorded in years 2010 (1.7) and 2016 (1.9).

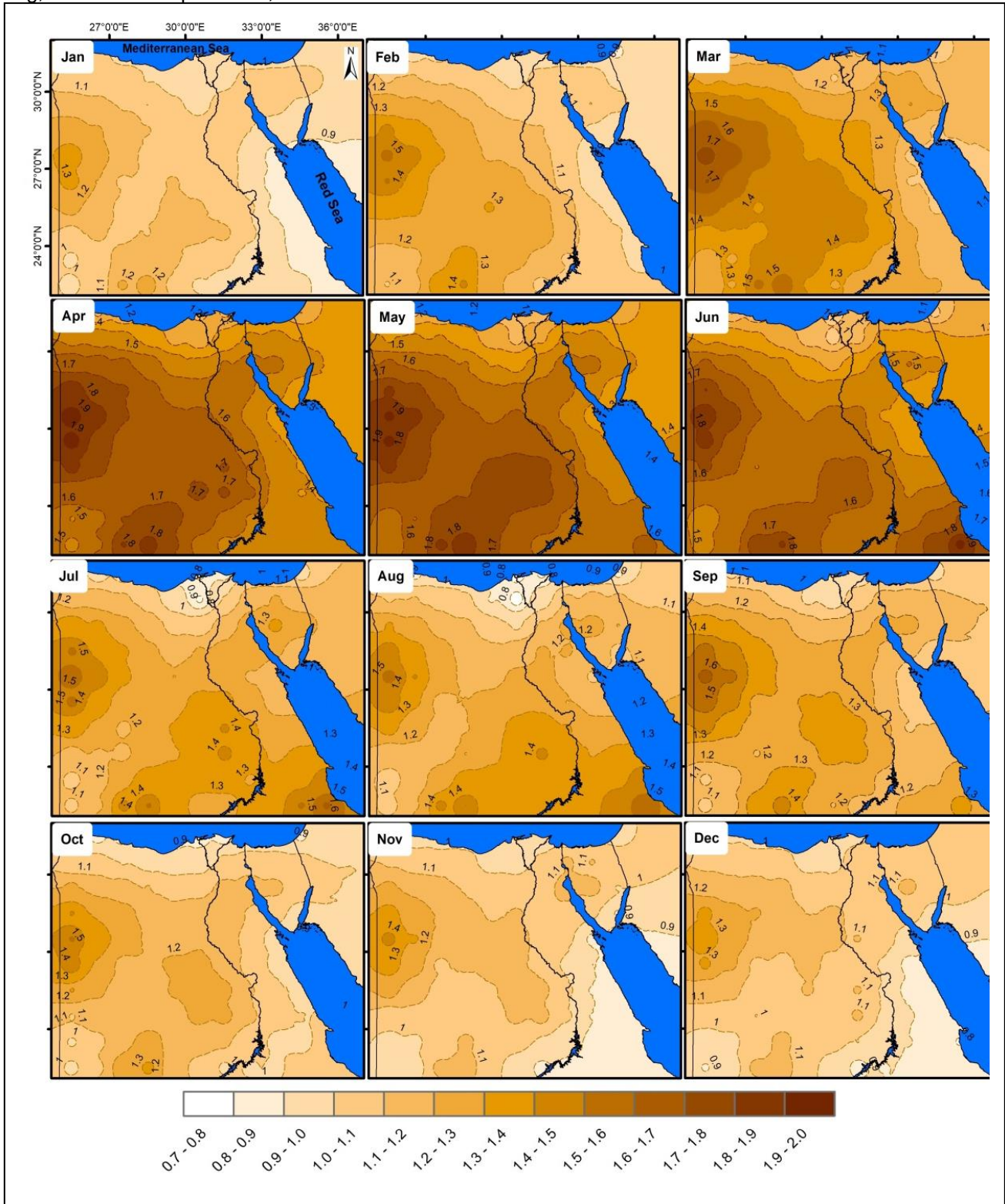


Fig. 8. Spatial distribution of Monthly average OMI-AI over Egypt (2005 to 2016).

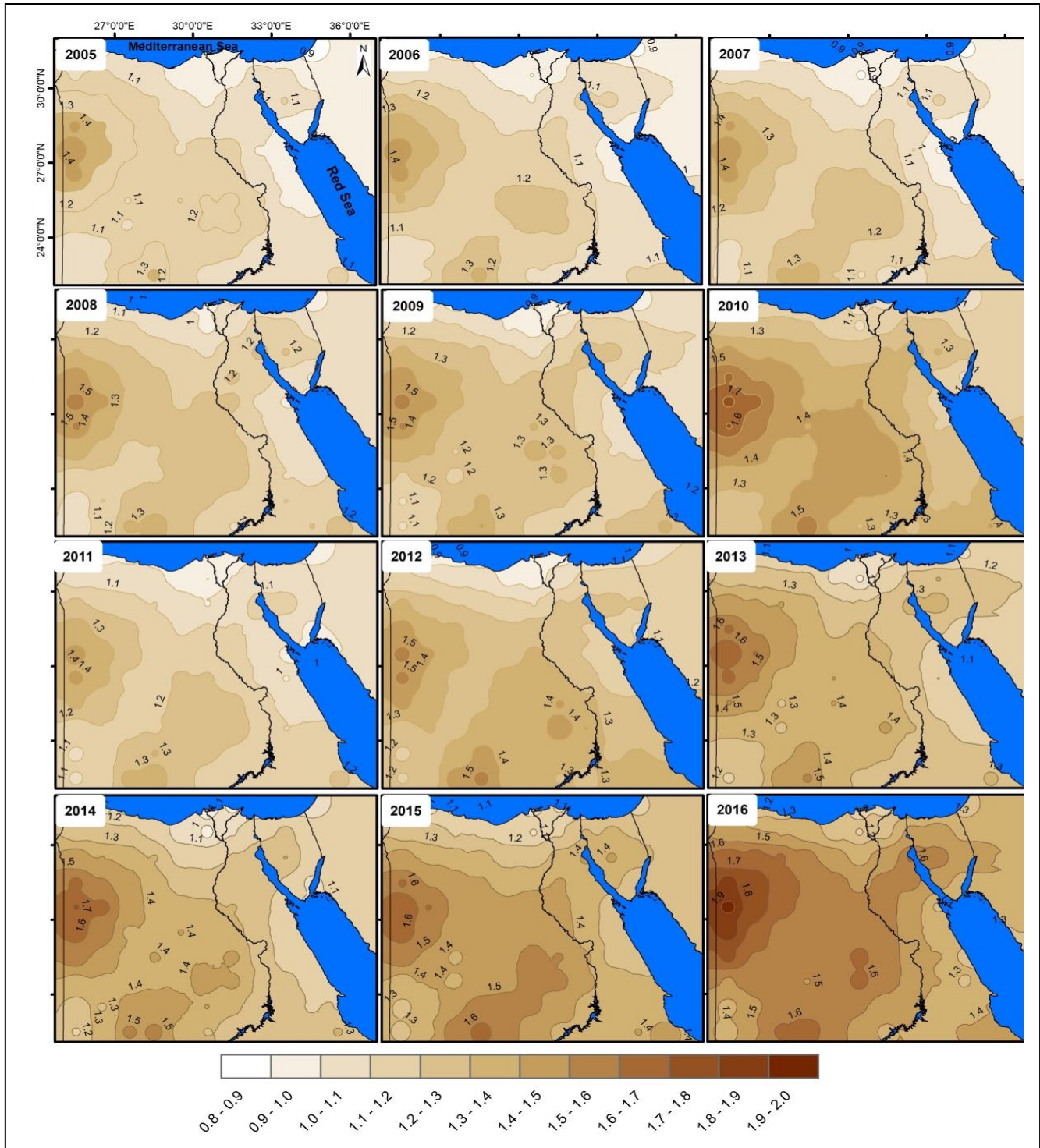


Fig. 9. Spatial distribution of annual average OMI-AI over Egypt (2005 to 2016).

**E. Correlation coefficients between OMI-AI and longitude**

The OMI-AI spatial distributions over Egypt show a pronounced east-to-west gradient. In order to analyze it we concentrate on the longitudinal variation of the OMI-AI values, spatially over the latitudinal 27.5°N. The monthly-mean longitude averaged OMI-AI values are plotted against longitude for each month, cold season, hot season and all period of the study (2005 –

2016) are analyzed, as shown in Fig. 10, with a linear fit of the form  $OMI-AI = a \cdot Lon + b$  where  $a$  and  $b$  values associated with the  $R^2$  coefficient are given in Table 1. Correlation coefficients ( $R^2$ ) between OMI-AI and Longitude are between 70% in February and 28% in November. Note also low  $R^2$  values in all period (29%), Cold season (40%) and Hot season (32%) indicative of large scatter. The slopes is (from -0.0447 to -0.0773) always negative, indicating a decreasing OMI-AI trend to the eastern longitudes.

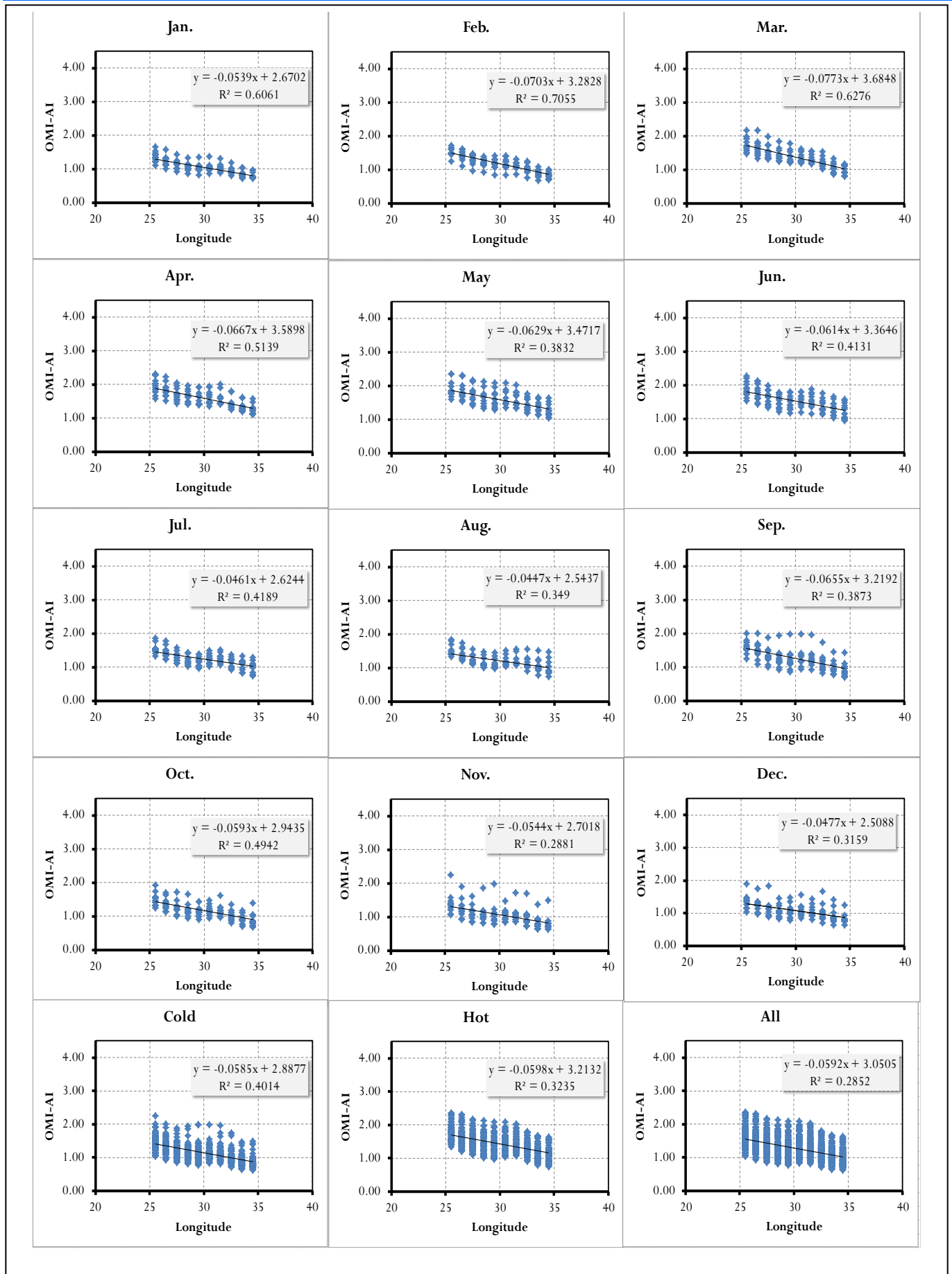


Fig. 10. Scatter Plot of the equation  $OMI-AI = a \cdot Lon + b$  and its correlation coefficient  $R^2$  over the mean latitudinal region  $27.5^\circ N$  correspond to each month, cold season, hot season and all the period (2005–2016) over Egypt.

TABLE I. VALUES OF THE A AND B COEFFICIENTS IN THE EQUATION  $OMI-AI = A * LONG + B$  AND ITS CORRELATION COEFFICIENT  $R^2$  OVER THE MEAN LATITUDINAL REGION  $27.5^{\circ}N$  CORRESPOND TO EACH MONTH, COLD SEASON, HOT SEASON AND ALL THE PERIOD (2005 – 2016) OVER EGYPT.

Period	Eq. $OMI-AI = a * Long + b$	$R^2$
January	$OMI-AI = -0.0539 * Long + 2.6702$	0.61
February	$OMI-AI = -0.0703 * Long + 3.2828$	0.71
March	$OMI-AI = -0.0773 * Long + 3.6848$	0.63
April	$OMI-AI = -0.0667 * Long + 3.5898$	0.51
May	$OMI-AI = -0.0629 * Long + 3.4717$	0.38
June	$OMI-AI = -0.0614 * Long + 3.3646$	0.41
July	$OMI-AI = -0.0461 * Long + 2.6244$	0.42
August	$OMI-AI = -0.0447 * Long + 2.5437$	0.35
September	$OMI-AI = -0.0655 * Long + 3.2192$	0.39
October	$OMI-AI = -0.0593 * Long + 2.9435$	0.49
November	$OMI-AI = -0.0544 * Long + 2.7018$	0.29
December	$OMI-AI = -0.0477 * Long + 2.5088$	0.32
Cold season	$OMI-AI = -0.0585 * Long + 2.8877$	0.40
Hot season	$OMI-AI = -0.0598 * Long + 3.2132$	0.32
All Period	$OMI-AI = -0.0592 * Long + 3.0505$	0.29

#### CONCLUSION

12-years (2005 to 2016) Spatial-Temporal Variability of OMI-AI over Egypt ( $22^{\circ}$ – $31^{\circ}N$ ,  $24^{\circ}$ – $36^{\circ}E$ ) were analyzed. Daily time series OMI-AI variations reflect increase with the time, daily average variation has generally high values during hot seasons, and low values during cold seasons. Daily OMI-AI average spatial distribution over Egypt is mapped onto a grid of  $1^{\circ}$  in longitude by  $1^{\circ}$  in latitude. Notice that a significant match in spatial distribution. So, in order to analyze the OMI-AI east-to-west gradient over Egypt; we study the longitudinal variation (at lat.  $27.5^{\circ}N$ ) of the OMI-AI values. OMI-AI does not depend on longitude or latitude, but only the areas which are active dust sources. So, we examining longitudinal trends to present it in a scientific paper these detailed correlations are not wrong, but of minor importance; nobody can use such equations in order to estimate OMI-AI in a specific area.

#### ACKNOWLEDGMENT

I greatly would like to acknowledge the OMI science data support teams for providing the data via Giovanni website (<http://giovanni.gsfc.nasa.gov/>). I gratefully acknowledge Dr. M. Ismaeil, geology department, for useful help. I am grateful to reviewers and editor for their useful comments to improve the manuscript. Also I sincerely thank Miss Amira Abdel Samei for her help in improving the language of this manuscript.

#### REFERENCES

[1] N. C. Hsu, J. R. Herman, P. K. Bhartia, Sefor, C. J., Torres, O., Thompson, A. M., Gleason, J. F., Eck, T. F., and Holben, B. N. "Detection of biomass burning smoke from TOMS measurements", *Geophys. Res. Lett.*, 23(7), 745–748, 1996.

[2] J.R. Herman, P.K. Bhartia, O. Torres, Hsu, C., Sefor, C., Celarier, E., "Global distribution of UV-absorbing aerosols from Nimbus 7/TOMS data". *Journal of Geophysical Research* 102 (D14), 1997, 16911–16922.

[3] O. Torres, P. K. Bhartia, J. R. Herman, Z. Ahmad, and J. Gleason, "Derivation of aerosol properties from satellite measurements of backscattered ultraviolet radiation: theoretical basis", *J. Geophys. Res.*, 103(D14): 17099–17110, 1998. doi:10.1029/98JD00900.

[4] O. Torres, A. Tanskanen, B. Veihelmann, C. Ahn, R. Braak, Bhartia, P. K., Veeffkind, P., and Levelt, P.: "Aerosols and surface UV products from Ozone Monitoring Instrument observations: an overview", *J. Geophys. Res.*, 112, D24S47, doi:10.1029/2007JD008809, 2007.

[5] A.M. Diaz, P. Hernandez-Leal, J.P. Diaz, F. J. Exposito, "Relation between toms-ai and air masses in the northeast atlantic free troposphere", *Adv. Space Res. Vol. 32. No. 11*, pp. 2263-2268, 2003, doi: 10.1016/S0273-1177(03)00698-7.

[6] J.M. Haywood, and K. P. Shine, "The effect of anthropogenic sulfate and soot aerosol on the clear sky planetary radiation budget", *Geophys. Res. Lett.*, 22, 603-606, 1995

[7] P. E. Ardanuy, L. Kyle, and D. Hoyt, "Global relationships among the earth's radiation budget, cloudiness, volcanic aerosols, and surface temperatures", *J. Clim.*, 5, 1120-1139, 1992

[8] B. A. Bodhaine, "Aerosol absorption measurements at Barrow, Mauna Loa, and the southpole", *J. Geophys. Res.*, 100, 8967-8975, 1995.

[9] N. C. Hsu, J. R. Herman, and S.-C. Tsay, "Radiative impacts from biomass burning in the presence of clouds during boreal spring in southeast Asia", *Geophys. Res. Lett.*, 30, 1224, doi:10.1029/2002GL016485, 2003.

[10] M. de Graaf, P. Stammes, and E. A. Aben, A. "Analysis of reflectance spectra of UV-absorbing aerosol scenes measured by SCIAMACHY", *J. Geophys. Res.*, 112, D02206, doi:10.1029/2006JD007249, 2007.

[11] N. Hsu, J. Herman, O. Torres, B. Holben, D. Tanre, T. Eck, A. Smirnov, B. Chatenet, and F. Lavenu, "Comparisons of the TOMS aerosol index with Sun-photometer aerosol optical thickness" Results and applications, *J. Geophys. Res.*, 104(D6), 6269–6279, 1999.

[12] N. M. Mahowald, and J. Dufresne, "Sensitivity of TOMS aerosol index to boundary layer height" implications for detection of mineral aerosol sources, *Geophys. Res. Lett.*, 31, L03103, doi:10.1029/2003GL018865, 2004.

[13] M. de Graaf, P. Stammes, O. Torres, and R. B. A. Koelemeijer, "Absorbing Aerosol Index:

sensitivity analysis, application to GOME and comparison with TOMS", *J. Geophys. Res.*, 110, D01201, doi:10.1029/2004JD005178, 2005.

[14] M. J. M. Penning de Vries, S. Beirle, and T. Wagner, "UV Aerosol Indices from SCIAMACHY: introducing the Scattering Index (SCI)", *Atmos. Chem. Phys.*, 9, 9555–9567, 2009

[15] J.M. Prospero, P. Ginoux, O. Torres, S.E. Nicholson, T. Gill, "Environmental characterization of global sources of atmospheric soil dust identified with Nimbus 7 Total Ozone Mapping Spectrometer (TOMS) absorbing aerosol product". *Rev. Geophys.* 2002, 40. doi:10.1029/2000RG000095.

[16] C. Moulin, I. Chiapello, "Evidence of the control of summer atmospheric transport of African dust over the Atlantic by Sahel sources from TOMS satellites (1979–2000)", *Geophysical Research Letters* 31 (L02107). 2004.

[17] A.C Anuforom, L.E. Akeh, P.N. Okeke, F.E. Opara, "Inter-annual variability and long-term trend of UV-absorbing aerosols during Harmattan season in sub-Saharan West Africa", *Atmospheric Environment* 41, 2007, 1550–1559.

[18] R., Washington, M., Todd, N.J., Middleton, Goudie, A.S., "Dust-storm source areas determined by the total ozone monitoring spectrometer and surface observations". *Annals of the Association of American Geographers* 93 (2), 2003, 297–313.

[19] P., Alpert, P., Kishcha, A., Shtivelman, S.O., Krichak, J.H., Joseph, "Vertical distribution of Saharan dust based on 2.5-year model predictions". *Atmos. Res.* 70, 2004, 109–130.

[20] S., Engelstaedter, I., Tegen, and R. Washington, "North African dust emissions and transport". *Earth-Science Reviews*, 79, 2006, 73–100.

[21] D.G. Kaskaoutis, P.T. Nastos, P.G. Kosmopoulos, H.D. Kambezidis, S.K. Kharol, K.V.S. Badarinath; "The Aura–OMI Aerosol Index distribution over Greece", *Atmospheric Research* 98, 2010, 28–39.

[22] D.G.Kaskaoutis, H.D., Kambezidis, P.T., Nastos, P.G., Kosmopoulos, "Study on an intense dust storm over Greece". *Atmos. Environ.* 42, 2008, 6884–6896.

[23] A. Deroubaix, N. Martiny, I. Chiapello, B. Marticorena, "Suitability of OMI aerosol index to reflect mineral dust surface conditions: Preliminary application for studying the link with meningitis epidemics in the Sahel", *Remote Sensing of Environment* 133 (2013) 116–127, <http://dx.doi.org/10.1016/j.rse.2013.02.009>

[24] Goudie, A.S., Middleton, N.J., 2001. Saharan dust storms: nature and consequences. *Earth-Science Reviews* 56, 179–204.

[25] Hang Gao and Richard Washington, "The spatial and temporal characteristics of TOMS AI over

the Tarim Basin, China", *Atmospheric Environment* 43, 2009, 1106–1115.

[26] Q.X., Gao, Z.H., Ren, Z.Q., Li, C.R., Pu., "Analysis of dust storms over China using EP/TOMS remote sensing data". *Research of Environmental Sciences* 4 (in Chinese). 2005

[27] Torres, O., R. Decae, J. P. Veefkind, and G. de Leeuw "OMI aerosol retrieval algorithm, in OMI Algorithm Theoretical Basis Document: Clouds, Aerosols, and Surface UV Irradiance", vol. 3, version 2, OMIATBD-03, edited by P. Stammes, 2002, pp. 47–71, NASA Goddard Space Flight Cent., Greenbelt, Md. (Available at [http://eosps.gsfc.nasa.gov/eos\\_homepage/for\\_scientists/atbd/docs/OMI/ATBD-OMI-03.pdf](http://eosps.gsfc.nasa.gov/eos_homepage/for_scientists/atbd/docs/OMI/ATBD-OMI-03.pdf))

[28] Zhou, X.J., Li, W.G., Luo, Y.F., "Analysis of the 1980s atmospheric aerosol optical depth over China". *Journal of Applied Meteorological Science* 1 (in Chinese). 2001.

[29] J. F., Gleason, N. C., Hsu, and O. Torres.; "Biomass burning smoke measured using backscattered ultraviolet radiation: SCAR-B and Brazilian smoke interannual variability", *J. Geophys. Res.*, 103(D24), 1998, 31969–31978.

[30] M., Fromm, R., Bevilacqua, R., Servanckx, J., Rosen, Thayer, J. P., J., Herman, and Larko, D. "Pyrocumulonimbus injection of smoke to the stratosphere: Observations and impact of a super blowup in northwestern Canada on 3-4 August 1998" *J. Geophys. Res.*, 110, 2005, D08205, doi:10.1029/2004JD005350.

[31] M., Fromm, A., Tupper, D., Rosenfeld, R., Servanckx, and R. McRae, "Violent pyro-convective storm devastates Australia's capital and pollutes the stratosphere", *Geophys. Res. Lett.*, 33, L05815, 2006, doi:10.1029/2005GL025161.

[32] Zhao, F & Wang, W & Deng, X & Yang, Y & Peng, Y. "Relationship between absorbing aerosol index and total column ozone". *Yaogan Xuebao/Journal of Remote Sensing*. 21. 2017, 500-508. doi: 10.11834/jrs.20176324.

[33] S.P., Ahmad, O., Torres, P.K., Bhartia, G., Leptoukh, S.J., Kempler "Aerosol index from TOMS and OMI measurements" *Proceedings of the 86<sup>th</sup> AMS Annual Meeting*, February 2006.

[34] Salman Tariq, Muhammad Ali, "Spatio-temporal distribution of absorbing aerosols over Pakistan retrieved from OMI onboard Aura satellite", *Atmospheric Pollution Research* 6, 2015, 254-266.

[35] M., Abu-Allaban, A. W., Gertler, and D. H. Lowenthal, "A preliminary apportionment of the sources of ambient PM<sub>10</sub>, PM<sub>2.5</sub>, and VOCs in Cairo", *Atmos. Environ.*, 36, 2002, 5549–5557.

[36] M., Abu-Allaban, D. H., Lowenthal, A. W., Gertler, and M. Labib, "Sources of PM<sub>10</sub> and PM<sub>2.5</sub>

in Cairo's ambient air", *Environ. Monit. Assess.*, 133, 417–425, 2007, doi:10.1007/s10661-006-9596-8.

[37] A. S., Zakey, M. M., Abdelwahab, and P. A. Makar, "Atmospheric turbidity over Egypt", *Atmos. Environ.*, 38, 2004, 1579–1591.

[38] S. C. Alfaro, and M. A. Wahab, "Extreme variability of aerosol optical properties: The Cairo aerosol characterization experiment case study", *Nato. Sec. Sci.*, 285–299, 2006, doi:10.1007/978-1-4020-5090-9 18.

[39] H. El-Askary, and M. Kafatos, "Dust storm and black cloud influence on aerosol optical properties over Cairo and the greater delta region, Egypt", *Int. J. Remote Sens.*, 29, 2008, 7199–7211.

[40] O., Favez, H., Cachier, J., Sciare, S. C., Alfaro, T. M., El-Araby M. A., Harhash, and M. M. Abdelwahab, "Seasonality of major aerosol species and their transformations in Cairo megacity", *Atmos. Environ.*, 42, 2008, 1503–1516.

[41] K. F., Mahmoud, Alfaro, S. C., Favez, O., Abdel Wahab, M. M.: "Origin of black carbon concentration peaks in Cairo (Egypt)", *Atmos. Res.*, 89, 2008, 161–169.

[42] M., El-Metwally, S. C., Alfaro, M., Abdel Wahab, and B. Chatenet, "Aerosol characteristics over urban Cairo: Seasonal variations as retrieved from Sunphotometer measurements", *J. Geophys. Res.*, 113, D14219, 2008, doi:10.1029/2008JD009834.

[43] A. K., Prasad, H., El-Askary, and M. Kafatos, "Implications of high altitude desert dust transport from Western Sahara to Nile Delta during biomass burning season", *Environ. Pollut.*, 158, 2010, 3385–3391.

[44] H. S., Marey, J. C., Gille, H. M., El-Askary, E. A., Shalaby, and M. E. El-Raey, "Study of the formation of the "black cloud" and its dynamics over Cairo, Egypt, using MODIS and MISR sensors", *J. Geophys. Res.*, 115, 2010, D21206, doi:10.1029/2010JD014384.

[45] H. S. Marey, J. C. Gille, H. M. El-Askary, E. A. Shalaby, and M. E. El-Raey: Aerosol climatology over Nile Delta based on MODIS, MISR and OMI satellite data, *Atmos. Chem. Phys.*, 11, 10637–10648, 2011, doi:10.5194/acp-11-10637-2011.

[46] A. A. Abdallah, M. M. Eid, Abdel Wahab M. M. and F. M. El-Hussainy, "A Simulated Climatology of North African Dust and its Impact on Meteorological Parameters Using WRF-CHEM Model", *International Journal of Advanced Research*, Volume 3, Issue 1, 2016, 1011- 1023.

[47] P.F., E.Levelt, G. W. Hilsenrath, G. H. J. Leppelmeier, P. K. van den Oord, Bhartia, J. Tamminen, J. F. de Haan, and J. P. Veefkind, "Science objectives of the Ozone Monitoring Instrument, *IEEE Trans. Geosci. Remote Sens.*, 44(5), 2006, 1093–1101.

[48] P. F. Levelt, et al., "Science Objectives of EOS-Aura's Ozone Monitoring Instrument (OMI)", *Proc. Quad. Ozone Symposium*, Sapporo, Japan, 2000, pp. 127-128.

[49] S. P. Ahmad, P. F. Levelt, P. K. Bhartia, E. Hilsenrath, G.W. Leppelmeier, and J. E. Johnson, "Atmospheric Products from the Ozone Monitoring Instrument (OMI)", *Proceedings of SPIE conference on Earth Observing Systems VIII*, Volume 5151pp 619630. (<http://acdisc.gsfc.nasa.gov/ozone/docs/omi-spie 2003.doc>), 2003.

[50] Jing Li, Barbara E. Carlson, and Andrew A. Lacis "A study on the temporal and spatial variability of absorbing aerosols using Total Ozone Mapping Spectrometer and Ozone Monitoring Instrument Aerosol Index data", *J. GEOPHYSICAL RESEARCH*, VOL.114,, 2009 D09213, doi:10.1029/2008JD011278.

[51] S. Engelstaedter, I. Tegen, and R. Washington "North African dust emissions and transport", *Earth-Science Reviews* 79(1):73-100, 2006 DOI:10.1016/j.earscirev.2006.06.004.

[52] C., Moulin, C.E., Lambert, U., Dayan, Masson, V., Ramonet, M., Bousquet, P., Legrand, M., Balkanski, Y.J., Guelle, W., Marticorena, B., Bergametti, G., Dulac, F., "Satellite climatology of African dust transport in the Mediterranean atmosphere". *Journal of Geophysical Research*, [Atmospheres] 103 (D11), 13, 1998, 137–13, 144.

[53] S. Guerzoni, E. Molinaroli, R. Chester, Saharan dust inputs to the western Mediterranean Sea: depositional patterns, geochemistry and sedimentological implications, *Deep Sea Research Part II: Topical Studies in Oceanography*, Volume 44, Issues 3–4, 1997, Pages 631-654, ISSN 0967-0645, [https://doi.org/10.1016/S0967-0645\(96\)00096-3](https://doi.org/10.1016/S0967-0645(96)00096-3).

[54] Prospero, J.M., Nees, R.T., "Impact of the North African Drought and El-Nino on mineral dust in the Barbados trade winds". *Nature* 320 (6064), 735–738, 1986.

[55] Perry, K.D., Cahill, T.A., Eldred, R.A., Dutcher, D.D., Gill, T.E. " Long-range transport of North African dust to the eastern United States". *Journal of Geophysical Research*, [Atmospheres] 102(D10), , 1997, 11, 225–11, 238.

[56] Prospero, J.M., "Assessing the impact of advected African dust on air quality and health in the eastern United States". *Human and Ecological Risk Assessment* 5 (3), 1999, 471–479.

[57] M., El-Metwally, S. C., Alfaro, M. M., Abdel Wahab, Zakey, A. S., and Chatenet, B. "Seasonal and inter-annual variability of the aerosol content in Cairo (Egypt) as deduced from the comparison of MODIS aerosol retrievals with direct AERONET measurements", *Atmos. Res.*, 97, 2010, 14–25.